Available online at www.sciencedirect.com
ScienceDirect
International Journal of Heat and Fluid Flow 28 (2007) 1312–1326
International Journal of HEAT AND FLUID FLOW
www.elsevier.com/locate/ijhff

Evolution of jets effusing from inclined holes into crossflow

W. Jessen *, W. Schröder, M. Klaas

Chair of Fluid Mechanics Institute of Aerodynamics, RWTH Aachen University, Wüllnerstraße zw. 5 and 7, D-52062 Aachen, Germany

Received 22 December 2006; received in revised form 12 June 2007; accepted 29 June 2007
Available online 20 August 2007

Abstract

The turbulent flow structure and vortex dynamics of a jet-in-a-crossflow (JICF) problem, which is related to gas turbine blade film cooling, is investigated using the particle-image velocimetry (PIV) technique. A cooling jet emanating from a pipe interacts with a turbulent flat plate boundary layer at a Reynolds number $Re_\infty = 400{,}000$. The streamwise inclination of the coolant jet is 30° and two velocity ratios (VR = 0.28, VR = 0.48) and two mass flux ratios (MR = 0.28, MR = 0.48) are considered. Jets of air and CO_2 are injected separately into a boundary layer to examine the effects of the density ratio between coolant and mainstream on the mixing behavior and consequently, the cooling efficiency. The results show a higher mass flux ratio to enlarge the size of the recirculation region leading to a more pronounced entrainment of hot outer fluid into the wake of the jet. Furthermore, the lateral spreading of the coolant is strongly increased at a higher density ratio. The results of the experimental measurements are used to validate numerical findings. This comparison shows an excellent agreement for mean velocity and higher moment velocity distributions.

Keywords: Film cooling; Velocity ratio; Density ratio; Mass flux ratio; Particle-image velocimetry (PIV)

1. Introduction

To improve the efficiency of gas turbine engines the gas inlet temperature has to be increased beyond the failure temperature of the turbine blade and vane material. In other words, gas turbine blades have to be protected from the hot gases using a thin fluid film that is wrapped around the blade. To achieve such a protective layer cooler air is injected through discrete holes on the blade surface.

This problem has been analyzed by numerous numerical and experimental studies like, e.g., Guo et al. (2006), Renze et al. (in press), Walters and Leylek (2000) and Baldauf et al. (2001). The experiments, however, used intrusive techniques such as hotwires, cold wires, and thermocouples to obtain local, time resolved point measurements of the velocity, temperature, and mixing of the film-cooling mechanism. With these measurement methods the spatial structure of the flow field of a jet emanating from a hole into a turbulent boundary layer can only be resolved on a point by point basis. A better spatial resolution of the flow field can be achieved by the particle-image velocimetry (PIV) technique that has been used by Peterson and Plesniak (2004) and David et al. (2004) to study flow structures like the counter-rotating vortex pair (CVP) or wake vortices that appear in a JICF problem. Most of the PIV investigations as for instance Jovanovic et al. (2006) consider variations of parameters like the Reynolds number, blowing ratios, and the influence of jet shapes in a range that is relevant for the cooling process. However, the density difference between the coolant and the crossflow that appears in a gas turbine engine due to the temperature ratio is only considered in a recent publication by Bernsdorf et al. (2006), who discussed mean flow measurements but no turbulence statistics.

It is evident that experimental investigations of turbine blade flows at real temperatures, i.e., in the range of $1300 \leqslant T_G \leqslant 1600$ K, require extremely complex and expensive wind tunnel equipment. To circumvent problems due to the high temperatures investigations of effects of density differences between the coolant and the crossflow through the use of a denser cooling gas were carried out.

* Corresponding author. Tel.: +49 241 80 94358; fax: +49 241 80 92257.
E-mail address: w.jessen@aia.rwth-aachen.de (W. Jessen).

0142-727X/$ - see front matter © 2007 Elsevier Inc. All rights reserved.
doi:10.1016/j.ijheatfluidflow.2007.06.010

Nomenclature

D	cooling hole diameter
DR	jet-to-mainstream density ratio $= \rho_j/\rho_\infty$
f	mixing fraction $= \rho_n/\rho_{tot}$
H	vertical distance between the surface of the plate and the top of the chamber
IR	jet-to-mainstream momentum ratio $= \rho_j u_j^2/\rho_\infty u_\infty^2$
MR	jet-to-mainstream mass flux ratio $= \rho_j u_j/\rho_\infty u_\infty$
Re_∞	local Reynolds number based on the distance from the leading edge
R_Θ	momentum thickness Reynolds number at the point of injection
H_{12}	shape factor at the point of injection
u_j	jet velocity
u'_{rms}	streamwise fluctuation velocity
u_∞	streamwise mean velocity
VR	jet-to-mainstream velocity ratio $= u_j/u_\infty$
X	streamwise distance based on hole center line
Y	vertical distance based on hole center line
Z	spanwise distance based on hole center line
δ	boundary-layer thickness
ρ	density

Subscripts

j	jet conditions
n	species index
∞	mainstream conditions
rms	root mean square
tot	total

The first experimental studies investigating the density influence on a film-cooling problem has been done by Goldstein and Eckert (1974) using Freon vapor to provide a denser coolant. A mixture of air and CO_2 was injected into the mainstream by Petersen et al. (1977). Adiabatic wall measurements showed that the film-cooling effectiveness through jet injection strongly depends on the density ratio. Teekaram et al. (1989) investigated CO_2 injections into the main air stream at two temperature conditions, i.e., two density ratios (DR = 1.25, DR = 1.67) were analyzed. The obtained heat transfer results showed a close agreement between the results of the injection to mainstream density ratios achieved either by changing the injection to mainstream temperature ratio or by using a foreign gas injection. Han and Mehendale (1986) studied the effect of the blowing ratio at an air and steam injection. Pietrzyk et al. (1990) conducted measurements in the flow field that resulted from cooling the air jet to obtain a density ratio of DR = 2. These measurements were carried out in the vicinity of the exit holes by means of the Laser-Doppler anemometry technique (LDA). In addition, Sinha et al. (1991) injected a cooled air stream into a crossflow and found that an increase in the coolant to mainstream density ratio leads to an improved film-cooling effectiveness. Mehendale et al. (1994) reports about the effect of density ratio on blade film effectiveness and heat transfer distributions over a linear turbine cascade achieved from CO_2 injection to produce a density ratio of DR = 1.48. Ekkad et al. (1997) confirm the higher cooling effectiveness for the CO_2 jet emanating from simple angled holes compared to compound angle injection using the transient liquid crystal technique. Applying the same measurement technique Ekkad et al. (1998) found out that an increase in coolant density caused a decrease in heat transfer coefficients at all blowing ratios. The injection of CO_2 provided an injection to mainstream density ratio of DR = 1.5 with the highest effectiveness at MR = 0.8. They also obtained an increase in coolant density had little effect on film effectiveness distributions at higher blowing ratios. Focusing on the velocity and temperature fluctuation measurements using a cold wire in conjunction with LDA have been conducted by Kohli and Bogard (2005) producing a density ratio of DR = 1.05 to study the turbulent transport of heat in a film-cooling field.

As indicated above, there has hardly been any previous experimental study using the PIV technique to analyze simultaneous the velocity and density influence on the complex turbulent flow field of a JICF problem. In addition, the other investigations that considered density ratios between the jet and the crossflow were only carried out to examine the effects of jet density on the wall temperature or the flow field on a point by point basis. They have, however, failed to describe the density effect on the vortical structures present within these flow fields. This is of particular importance as these structures dictate the final development of the flow field patterns which in turn determine the mixing process and the cooling efficiency of the JICF.

In this paper the flow pattern resulting from such an air–CO_2 mixing process will be investigated and compared against the mixing behavior of an air jet injected into an air crossflow. The turbulent flow structure and vortex dynamics that influence the cooling efficiency depend strongly on the velocity and density ratio. The measurements allow a detailed analysis of such a flow field and are used to validate numerical data presented in Guo et al. (2006) and Renze et al. (in press).

The organization of the paper is as follows: First a brief description of the experimental setup, the flow conditions and the measurement technique is given. Subsequently, the flow structure in different measurement planes in which jets emanate into an air-like crossflow is analyzed considering different velocity and density ratios. This is followed by the discussion of the experimental results and finally a comparison with numerical data investigating the same JICF problem is made.

2. Experimental setup

The experiments were carried out in the low-speed wind tunnel of the Institute of Aerodynamics at the RWTH Aachen University. It is a Göttingen type wind tunnel with an open test section, which is 1.80 m long and has a cross sectional diameter of 1.2 m.

To investigate the JICF problem a horizontal plate with a symmetrical leading-edge nose has been installed in the measuring section of the wind tunnel. The boundary layer is tripped at the leading edge to generate a fully developed turbulent boundary layer similar to that found in typical film-cooling applications. The flat plate is equipped with an insert that contains a row of three holes from which the jets discharge at a streamwise angle of 30° into the turbulent boundary layer of the crossflow. To simulate the flow parameters in a gas turbine the local Reynolds number at the hole location is set according to Mehendale et al. (1994) at $Re_\infty = 400{,}000$ and the ratio of the local boundary-layer thickness to the hole diameter is $\delta/D = 2$. The momentum thickness based Reynolds number at the point of injection is $R_\Theta = 1086$ and the shape factor, i.e., the ratio of displacement thickness and momentum thickness, is $H_{12} = 1.49$. The inclined jet holes have a diameter of $D = 10$ mm each and are located three diameters apart. According to these flow parameters the turbulent boundary-layer thickness for a flat plate at the point of the injection has to be 20 mm. To achieve the desired flow parameters the distance from the leading edge to the centerline of the injection hole has to be $x = 713$ mm corresponding to Eq. (2) (see Fig. 1).

The jets are supplied through a plenum that is located underneath the plate and can be filled with either air or CO_2 to provide air or CO_2 jets. The vertical distance between the surface of the plate and the top of the chamber is chosen to be $H/D = 12$ that leads to a supply channel length of $24D$. These two geometry parameters are set to investigate effusion cooling through laser drilled holes with a diameter of 0.2 mm in full-scale. The velocity, density, mass flux, and momentum flux ratio are defined as

$$\mathrm{VR} = \frac{u_j}{u_\infty}, \quad \mathrm{DR} = \frac{\rho_j}{\rho_\infty}, \quad \mathrm{MR} = \frac{\rho_j u_j}{\rho_\infty u_\infty}, \quad \mathrm{IR} = \frac{\rho_j u_j^2}{\rho_\infty u_\infty^2}. \tag{1}$$

The subscripts j and ∞ denote the jet and crossflow fluid. The crossflow velocity is set according to the desired flow parameters to $u_\infty = 8.61$ m/s and the velocity ratios are $\mathrm{VR} = 0.28$ and $\mathrm{VR} = 0.48$. The jet-to-mainstream mass flux ratios are determined at $\mathrm{MR} = 0.28$ and $\mathrm{MR} = 0.48$. Two different values of the density ratio DR, an air-to-air injection with $\mathrm{DR} = 1$ and a CO_2-to-air injection with $\mathrm{DR} = 1.53$, are considered with both gases injected at the same temperature of 24 °C. Table 1 gives an overview of all considered blowing and density ratios.

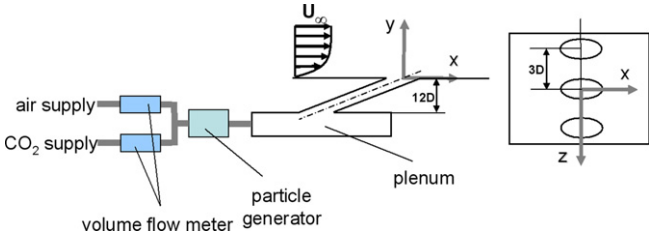

Fig. 1. Schematic of the air/CO_2 supply unit.

Table 1
Velocity, density, mass flux, and momentum flux ratios

	Air injection		CO_2 injection			
VR	0.28	0.48	0.18	0.28	0.31	0.48
DR	1	1	1.53	1.53	1.53	1.53
MR	0.28	0.48	0.28	0.43	0.48	0.73
IR	0.08	0.23	0.05	0.12	0.15	0.35

3. Measurement technique

Velocity and vorticity distributions are measured by the particle-image velocimetry (PIV) method. The measurements are typically performed for the central hole. Two component (2C) and three component (3C) PIV techniques have been used in different planes parallel and perpendicular to the surface of the flat plate to determine the velocity and vorticity distributions in the jet and the freestream flow.

The PCO Sensicam-CCD cameras used for the PIV measurements have a resolution of 1280×1024 pixels and a dynamic range of 16 bit. In order to determine the flow field around and downstream the jet exit with the same resolution, the 2C-PIV arrangement consists of two CCD cameras that are positioned next to each other perpendicular to the measurement plane. The 3C-PIV setup compromises two CCD cameras arranged under the Scheimpflug-condition with an optimum angle of ±45° between the axis of the lenses and the measured plane. The light sheet is generated by double pulsed Nd:YAG-lasers each with a power rating of 25 mJ. The light sheet optics creates a light sheet in the area of interest with a thickness of 1 mm. The cameras and the light sheet are controlled by an external synchronizer operated at a frequency of 2 Hz. Typical time intervals between images within a pair were 20–40 μs. Two Nikon lenses with a focal length of 80–200 mm and an aperture value of 1/2.8 are used. Fig. 2 gives an overview of the general 3C-PIV arrangement, the open test section, and the flat plate with the position of the insert where the jets emanate.

The jets and the free stream were seeded with 2–4 μm particles of solvent di-ethyl-hexyl-sebakat (DEHS) produced by two separate seeding generators.

To verify that the appropriate settings for the wind tunnel and the PIV system are used, trial measurements of 20–40 pairs of images were captured and processed. Four hundred image pairs were acquired for each experimental configuration, which after post-processing were

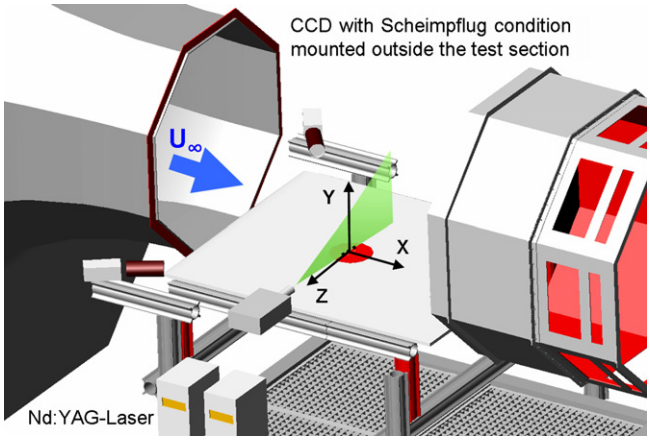

Fig. 2. Sketch of the 3C-PIV setup showing the location of the jet exit and the coordinate system.

temporally averaged to obtain the final velocity data. A separate measurement taking up to eight hundred image pairs showed no significant improvement of the mean velocity data.

Fig. 3 shows the planes at which 2C- and 3C-PIV measurements were taken. The 2C-PIV measurements were conducted in the X–Y plane at $z = 0$ mm in order to examine the extent of jet penetration and the properties of the recirculation regions beneath the jets for different flow conditions. Fig. 3b and c illustrates the X–Z and Y–Z planes at which the 3C-PIV measurements were conducted, respectively. The results obtained from these measurements were used to study the spanwise spread of the jets and to verify the level of jet penetration as observed from the 2C results.

The PIV evaluation process is done using the in-house written software Particle Image Analyzer (PIA). The typical interrogation window size is set at 32×32 pixels with an overlap of 50% that allows a spatial resolution of the measurement area of 0.63×0.63 mm^2. Each instantaneous vector field consists of 80×64 vectors, which generate more than 5000 data points.

No pre-filtering of bitmaps was done. The recorded size of the seeding particles is 1.5–2.8 pixels. The cross-correlation results of the 2C PIV measurements indicated in their instantaneous vector fields less than 0.04% erroneous vectors. These erroneous vectors were removed by post-procession using a local moving average validation over 3×3 vectors with acceptance factors of $k_1 = 0.4$ and $k_2 = 4$ according to Meinhart et al. (1994) as local neighborhood validation. These values for k_1 and k_2 proved to remove all erroneous vectors without affecting the valid vectors.

4. Experimental uncertainties

In the above described routines of the PIV measurements the sub-pixel accuracy of 0.01–0.015 pixels yields the minimum relative accuracy of approximately 0.5% in determining the velocity distributions close to the wall. The relative accuracy is higher at the boundary-layer edge since the mean particle displacement is approximately 7 pixels. At the achievable accuracy of 0.01–0.015 pixels the velocity at the boundary-layer edge can be determined with a maximum relative error of 0.15% such that the boundary-layer thickness $\delta_{0.99}$ is sufficiently accurately determined.

It is estimated that the laser sheet reflections distorted the near-wall velocity vector maps below $y = 0.2$ mm for the 2C- and $y = 0.4$ mm for the 3C PIV measurements. That is, the vector maps could possess a slight deviation from the accurate representation of the flow in this region.

To obtain identical conditions to compare the results of the injections of the two coolants in one measurement plane the arrangement of the air and CO_2 supply allowed to switch from air to CO_2 or vice versa without changing the PIV configuration or interrupting the main flow in the wind tunnel.

The uncertainty in the crossflow velocity was within a range of $\pm 1.5\%$ while that of the jet injections at any selected blowing ratio was $\pm 2\%$ due to the accuracy of the volume flux meters. Leak tests were conducted using an additional flow rate meter at the entrance of the plenum to ensure the mass flow entering the plenum to be exhausted only through the cooling holes. The results showed no losses in the flow rates at which the jets were emanated, although the whole setup of the coolant injection consisted of several tubes and connecting pieces. The pressurized air and CO_2 are exhausted through pressure regulators that keep both gases on a constant pressure, i.e., no pressure fluctuations occur during the measurements. Furthermore, the temperature was permanently measured using a digital thermometer inside the plenum. During a time span of three minutes, the time it takes to record 400 image pairs with the PIV setup, the temperature showed no measurable change at all velocity and mass flux ratios. The reason for the constant temperature inside the plenum is the large distance between the plenum and the jet exit via tubes and connecting pieces. Especially the passage of the gas through the liquid DEHS inside the particle generator at laboratory temperature (24 °C) ensures no significant temperature difference between the emanating

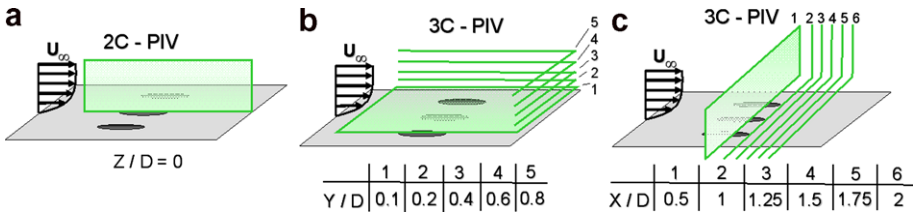

Fig. 3. Planes of 2C- and 3C-PIV measurements.

CO_2 and the crossflow to appear. Nevertheless, the temperature of the main flow in the wind tunnel increased by approximately 1–3 °C after a series of measurements and causes fluctuations in the density ratios in a range of ±1.4%.

5. Results

To determine the boundary-layer thickness 2C-PIV measurements were conducted in the X–Y plane on a flat plate, i.e., without a cooling jet hole. The measured X–Y plane was located at $z = 0$. The velocity distribution of the boundary layer was determined at the $x = 0$ position, which corresponds to the centerline of the inclined cooling hole.

Fig. 4a shows the time-averaged flow field on the flat plate without jet injection and Fig. 4b evidences the velocity distribution of the turbulent boundary layer being measured in the center plane at $x = 0$. The turbulent boundary-layer thickness is estimated using the classical relationship

$$\frac{\delta(x)}{x} = \frac{0.37}{(Re_x)^{1/5}}. \tag{2}$$

To achieve the required boundary-layer thickness of 20 mm, the distance from the leading edge of the flat plate to the centerline of the injection hole is 713 mm.

The velocity field obtained from the 2C-PIV measurements in the X–Y-center plane is presented for an air and a CO_2 injection in Fig. 5. To show the density influence of a jet-a-crossflow problem the velocity ratio VR = 0.28 and the mass flux ratio MR = 0.28 are considered. The velocity fields in Fig. 5 illustrate the effect of the inclined jet entering the boundary layer of the crossflow.

The streamwise velocity distribution above the boundary layer indicates that even at low velocity and mass flux ratios the freestream is affected. In this area the freestream is decelerated upstream of the injection area and then accelerated downstream of this cross section. The trajectory and the penetration of the coolant jet into the boundary layer are evidenced by the streamlines which start upstream of the leading edge of the cooling hole near the wall.

The comparison of the air and CO_2 injection at VR = 0.28 (Fig. 5a and b) demonstrates only slight deviations in the flow field pattern. There seems to be no difference between the penetration of the CO_2 jet into the boundary layer compared to the air jet at the same velocity ratio. The extent of the observed reverse flow region directly downstream of the injection hole has about the same size for both jets. The influence of the density difference gets more evident if the injections are considered at the mass flux ratio MR = 0.28 (Fig. 5a and c). The jet intrusion into the boundary layer of the CO_2 jet is about 30% lower than the air injection at MR = 0.28. Moreover, the reverse flow region in the wake of the jet can not be detected anymore. The cooling jet is deflected by the main flow immediately above the exit hole and reattaches directly downstream of the trailing edge without deeply penetrating into the boundary layer.

Fig. 6 shows the streamwise velocity distributions for the velocity and mass flux ratios of VR = 0.48 and MR = 0.48. At the higher velocity ratio VR = 0.48 the air and CO_2 jets penetrate clearly deeper into the crossflow than in the VR = 0.28 case. Although the velocity ratio has been increased there are no significant differences between the air and CO_2 jets entering the turbulent boundary layer (Fig. 6a and b). The dimension of the recirculation region immediately downstream of the injection hole possesses approximately the same size for both gases. Unlike these findings the comparison of the air and CO_2 injections at the mass flux ratio MR = 0.48 shows clear differences in the flow field patterns (Fig. 6a and c). The most obvious result is the lower intrusion of the CO_2 jet into the boundary layer compared to the air jet. Like in the lower mass flux ratio case the penetration of the denser jet is 30% smaller than at air injection. Nevertheless, the higher mass flux

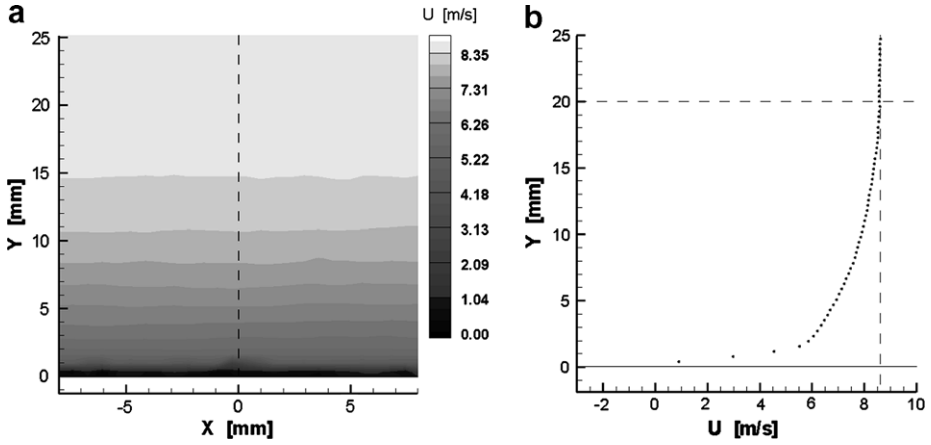

Fig. 4. Streamwise velocity contours in the X–Y-center plane at $z = 0$ without jet injection (a), velocity distribution of the turbulent boundary layer at $x = 0$ (b).

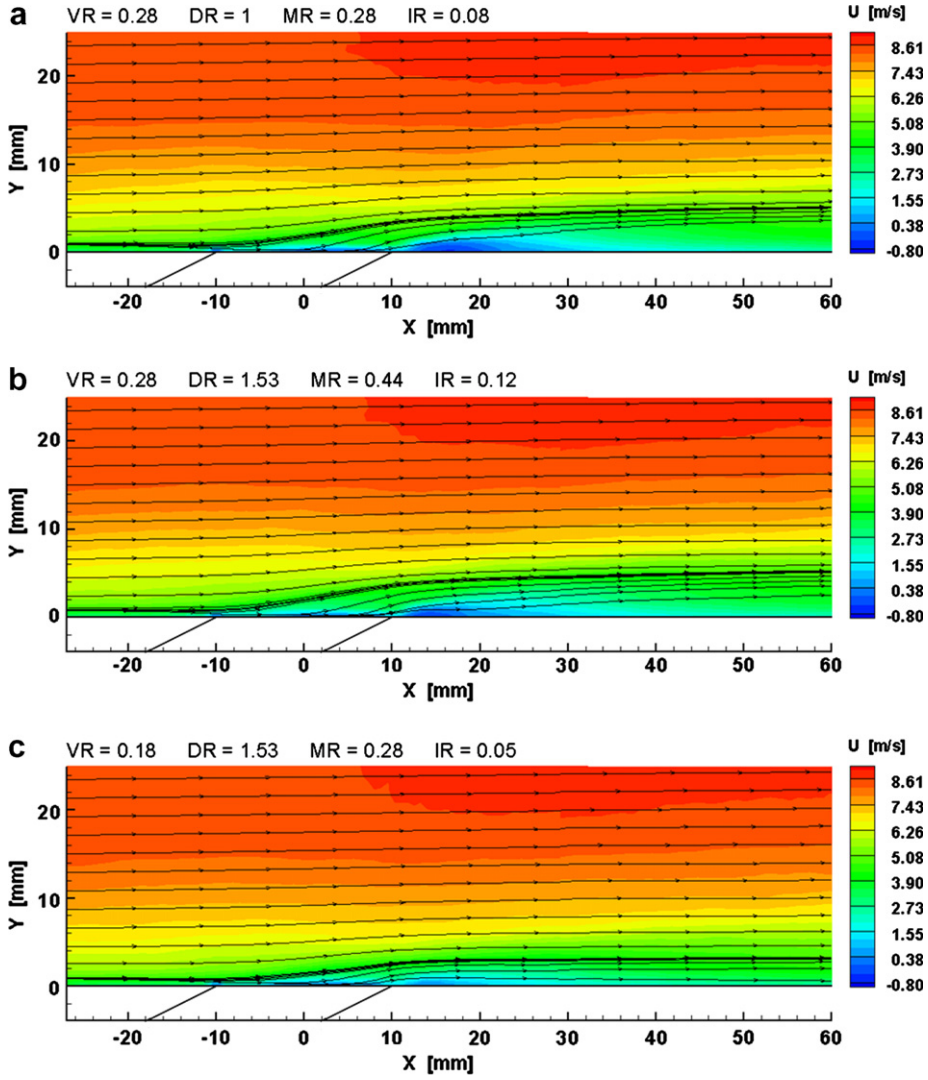

Fig. 5. Streamwise velocity distribution and streamlines in the X–Y-center plane for air injection at VR = MR = 0.28 (a), CO_2 injection at VR = 0.28 (b), and CO_2 injection at MR = 0.28 (c).

ratio yields a recirculation region in the wake of the denser jet. The size of this recirculation region is smaller and has lower reverse flow velocities compared to those being measured at DR = 1.

In Fig. 7 the recirculation regions downstream of the injection holes are shown in detail at all blowing ratios. The dashed lines indicate the streamwise extension of the regions where reverse flow appears. Both gases form a separation region at the velocity ratio VR = 0.28 downstream of the injection hole (Fig. 7a and b). The recirculation region of the air jet is larger compared to that of the CO_2 injection. A detailed analysis of the maximum mean velocities of the reverse flow shows higher values for the air injection ($u = -0.42$ m/s) than for the CO_2 injection ($u = -0.38$ m/s). No reverse flow can be detected in the leeward region of the injection hole at MR = 0.28 for the CO_2 jet (Fig. 7c). The impact of the recirculation in the wake region is clearly more pronounced when the velocity ratio is increased to VR = 0.48. At both gases the separation regions grow. The dimensions of these reverse flow regions are almost equal for the air and CO_2 injection at VR = 0.48 (Fig. 7d and e). The maximum mean velocities reached inside the recirculation regions are $u = -0.71$ m/s and $u = -0.63$ for the air and CO_2 jets, respectively. Unlike the lower mass flux ratio case also the CO_2 jet injected with a mass flux ratio of MR = 0.48 forms a reverse flow region in the jet wake (Fig. 7f). This reverse flow region is much smaller compared to those generated at the velocity ratio of VR = 0.48. The maximum mean velocity value being reached by the reverse flow is $u = -0.33$ m/s.

Regarding the cooling efficiency the jet penetrates at higher velocity and mass flux ratios deeper into the cross-flow leading to a larger recirculation region in the jet wake, where hot outer fluid might be entrained. The measurements of the CO_2 cases show that results based on the same temperature or density ratio between main flow and coolant are misleading since the size of the recirculation region and as such the cooling quality depend on the density

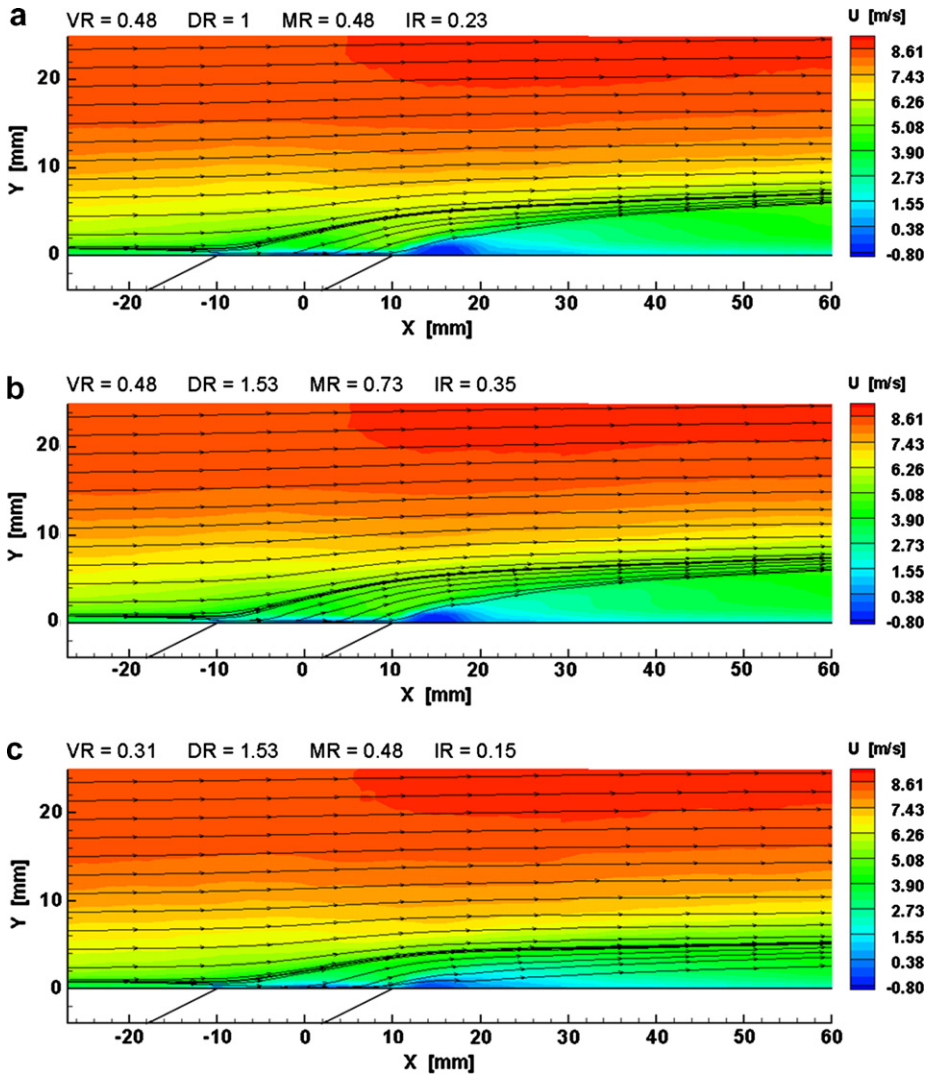

Fig. 6. Streamwise velocity distribution and streamlines in the X–Y-center plane for air injection at VR = MR = 0.48 (a), CO_2 injection at VR = 0.48 (b) and CO_2 injection at MR = 0.48 (c).

difference. This issue is clarified using the mass flux ratio instead of the velocity ratio although even when the velocity ratio is considered the density influence between a denser coolant jet and the crossflow is already detectable. The constant density assumption overestimates the dimension and the velocity values of the separation region and thus might result in a wrong efficiency prediction.

Fig. 8 shows the streamwise velocity distributions obtained for air and CO_2 injections at the velocity ratio VR = 0.48 at 1 mm and 2 mm above the surface of the plate. The most remarkable effect in the 1 mm plane is the different dimension of the recirculation region of the air and CO_2 jets situated downstream of the trailing edge of the hole (Fig. 8a and b). Although it was discussed in Fig. 7 that the reverse flow reaches its maximum below 1 mm it is clearly shown in Fig. 8 that the lateral extension of the CO_2 recirculation is much smaller compared to that of air. As a result of the lower density the deflection and constriction of the air jet caused by the main flow is more significant than that of the CO_2 jet. The lateral spreading of the CO_2 jet is already larger above the ejection hole and in the downstream area less constricted than the air jet. In the plane 2 mm above the plate the recirculation zones are no longer visible but the difference in the lateral spreading of the two different jets is still significant. The air jet appears to be much more slender in the spanwise direction. The velocity in the constricted part of the jet already reaches the magnitude of the non-affected crossflow. These findings show the obvious influence of the density on the cooling efficiency in the wake region with a larger extended area for the denser cooling jet.

The vorticity component $\omega_y = \partial u/\partial z - \partial w/\partial x$ normal to the surface at VR = 0.48 is presented in Fig. 9 for the air and CO_2 injection. The differentials are approximated by a Richardson extrapolation according to Raffel et al. (1998) with an accuracy of 4% under these conditions. These results were also obtained from 3C-PIV investigations in the plane located 1 mm above the flat plate. The

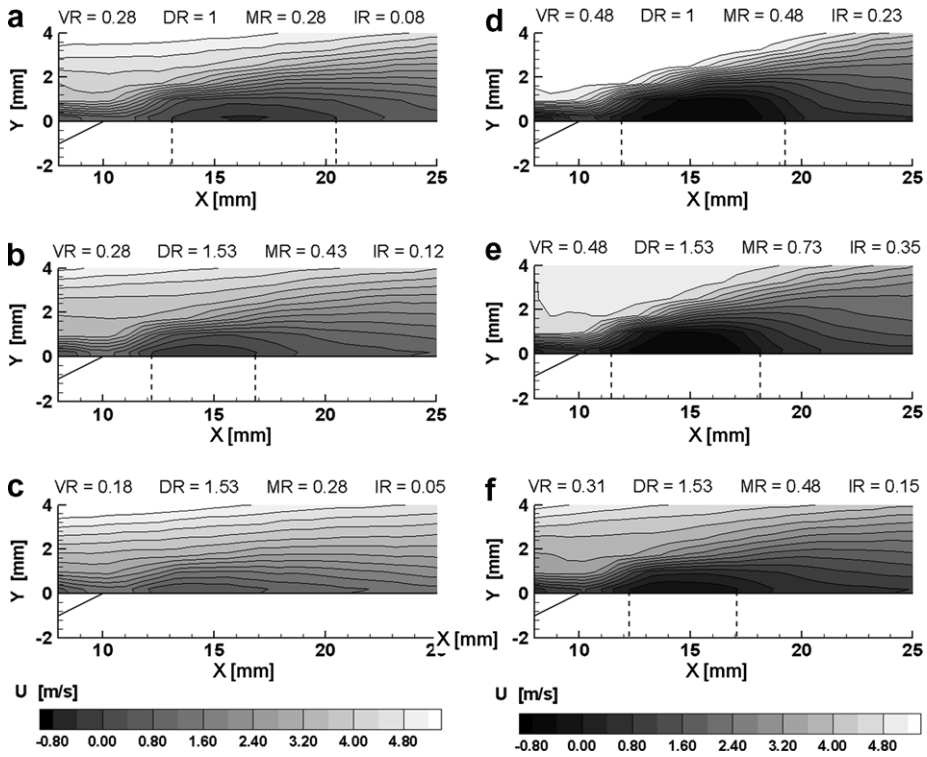

Fig. 7. Streamwise velocity contours in the X–Y-center plane in the wake region of the jet for air and CO_2 injection at several VR, DR, MR and IR values.

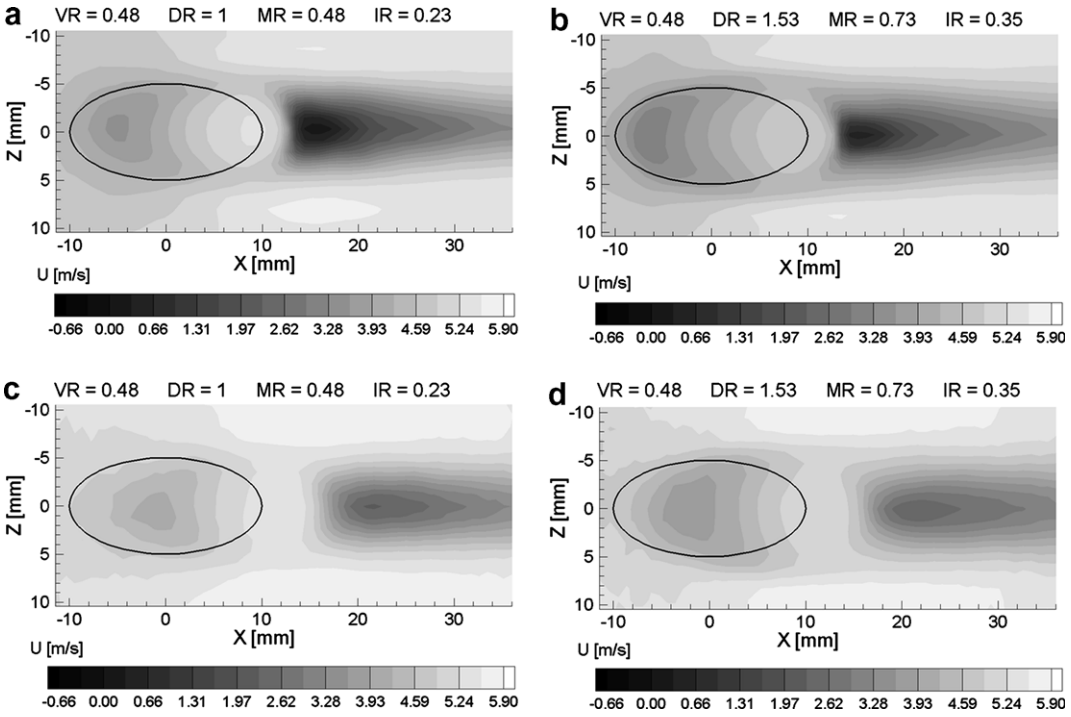

Fig. 8. Velocity contours at VR = 0.48 in the X–Z-plane 1 mm above the plate (air injection (a), CO_2 injection (b)) and 2 mm above the plate (air injection (c), CO_2 injection (d)); the flow is from left to right and the hole is indicated by the solid line.

vorticity of the CVP penetrating into the plane on the lee-side of the jet hole is evidenced. The regions of maximum vorticity of the air injection (Fig. 9a) are larger and more elongated compared to those of the CO_2 injection (Fig. 9b). As a result of the lower density the deflection and constriction of the air jet caused by the main flow is

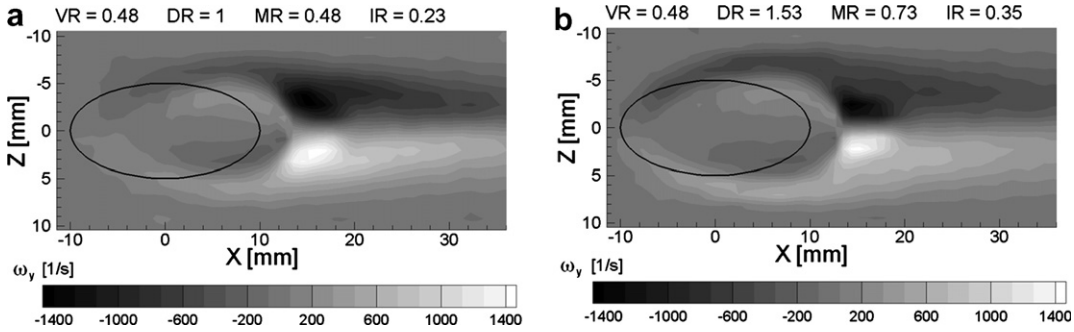

Fig. 9. Vorticity contours showing the vorticity ω_y in the X–Y plane 1 mm above the plate at VR = 0.48 (air injection (a), CO_2 injection (b)); the flow is from left to right and the hole is indicated by the solid line.

more significant than that of the CO_2 jet. Hence, it is clear that the density ratio has an influence on the jet penetration into the boundary layer and the lateral spreading downstream of the jet hole that affects the cooling efficiency.

The dominant flow structure in JICF problems is the counter-rotating vortex pair (CVP), which is known to have a detrimental effect on the film-cooling performance. 3C-PIV measurements were conducted to investigate the flow field in the spanwise direction in the wake region of the jet hole.

Fig. 10 shows the development of the CVP at the trailing edge of the exit hole ($X/D = 1$) for air and CO_2 injection by the velocity distribution based on the normal and spanwise velocity components in cross sections perpendicular to the wall. The normal velocity component is defined orthogonal to the flat plate surface. In the $X/D = 1$ plane the maximum velocity values are located in the spanwise symmetry plane. At VR = 0.48 the velocity distribution is similar for both density ratios (Fig. 10a and b). At about 2 mm from the centerline the flow starts to roll up to form a vortex on each side. Along the centerline the air injection produces higher mean velocity values normal to the wall than those of the CO_2 injection. The lower density jet is deflected earlier and the CVP develops faster, hence causing higher vertical velocities in the center. The vector distribution of the CO_2 injection extends further up in the flow field and confirms the higher penetration into the boundary layer of the cross-flow. As already stated above, the density influence

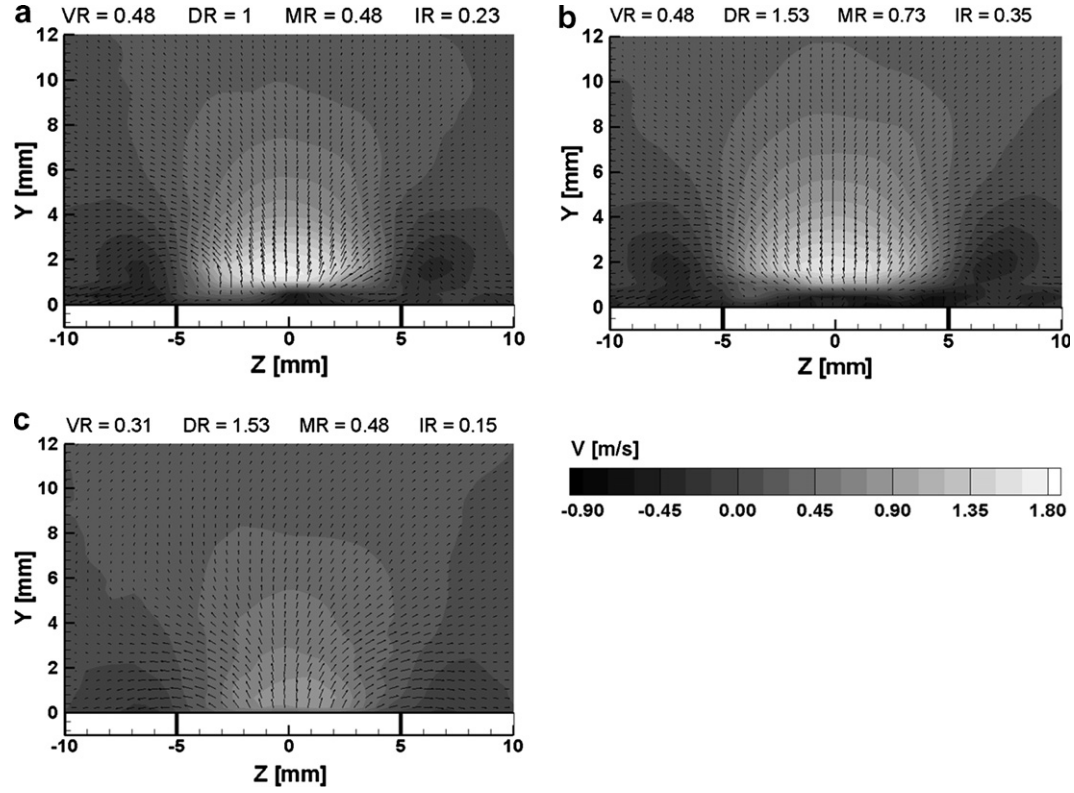

Fig. 10. Normal velocity contours and velocity field in the Y–Z-plane perpendicular to the wall at $X/D = 1$, air injection at VR = MR = 0.48 (a), CO_2 injection at VR = 0.48 (b) and CO_2 injection at MR = 0.48 (c).

becomes more evident when the mass flux ratio instead of the velocity ratio is considered for both injections. At MR = 0.48 the velocity contours for CO_2 indicate a smaller intrusion of the cooling jet into the boundary layer (Fig. 10c). Although the CO_2 jet intrusion at MR = 0.48 is of less intensity, the contours of a CVP forming already at the trailing edge of the hole can be observed. The CVP starts to roll up closer to the surface of the wall with nearly the same lateral extension as the CVP formed by the air jet.

The development of the CVP further downstream at the $X/D = 1.75$ plane is illustrated in Fig. 11. For both gases the vortices of the CVP at VR = 0.48 shift away from the wall and grow in size (Fig. 11a and b). Compared with Fig. 10 the vortices have migrated due to mutual induction. The spanwise distance between the vortex centers of the CO_2 jet is about 1 mm larger than that of the air jet. However, no significant difference in the lift-off distance is observed. In the CO_2 injection the vertical velocity near the centerline covers a larger region with higher values compared to the air injection. It seems that the denser vortices due to their larger size possess a higher vertical momentum flux. The flow field corresponding to the CO_2 jet at MR = 0.48 (Fig. 11c) differs from that of the air jet at MR = 0.48 and the CO_2 jet at VR = 0.48. The velocity contours show a weaker CVP and the region with maximum velocities is clearly smaller.

The quantitative comparison in Fig. 12 evidences the density influence and the development of the CVP by velocity profiles of the normal velocity component along the centerline measured at $X/D = 0$ and $X/D = 1.75$. Similar maximum mean velocities are reached for air and CO_2 injection if only the velocity ratio VR = 0.48 is considered for both injections. At the downstream edge of the jet hole ($X/D = 1$) the maximum mean velocities reach values for the air and CO_2 injection of $v = 1.69$ m/s and $v = 1.59$ m/s, respectively (Fig. 12a). When the mass flux ratio of MR = 0.48 is taken into account the maximum velocity value ($v = 0.83$ m/s) of the CO_2 jet is approximately 50% lower than that of the air jet. Further downstream at $X/D = 1.75$ the position of the maximum velocity has shifted away from the wall and the influence of the density difference is visible even in the velocity profiles of VR = 0.48 (Fig. 12b). The maximum value is now reached by the CO_2 injection at VR = 0.48 and appears to be 20% higher than that of the air injection.

Similarly to the results at $X/D = 1$ the velocity profile representing at MR = 0.48 for the CO_2 injection shows the same significant low velocity values compared to VR = 0.48.

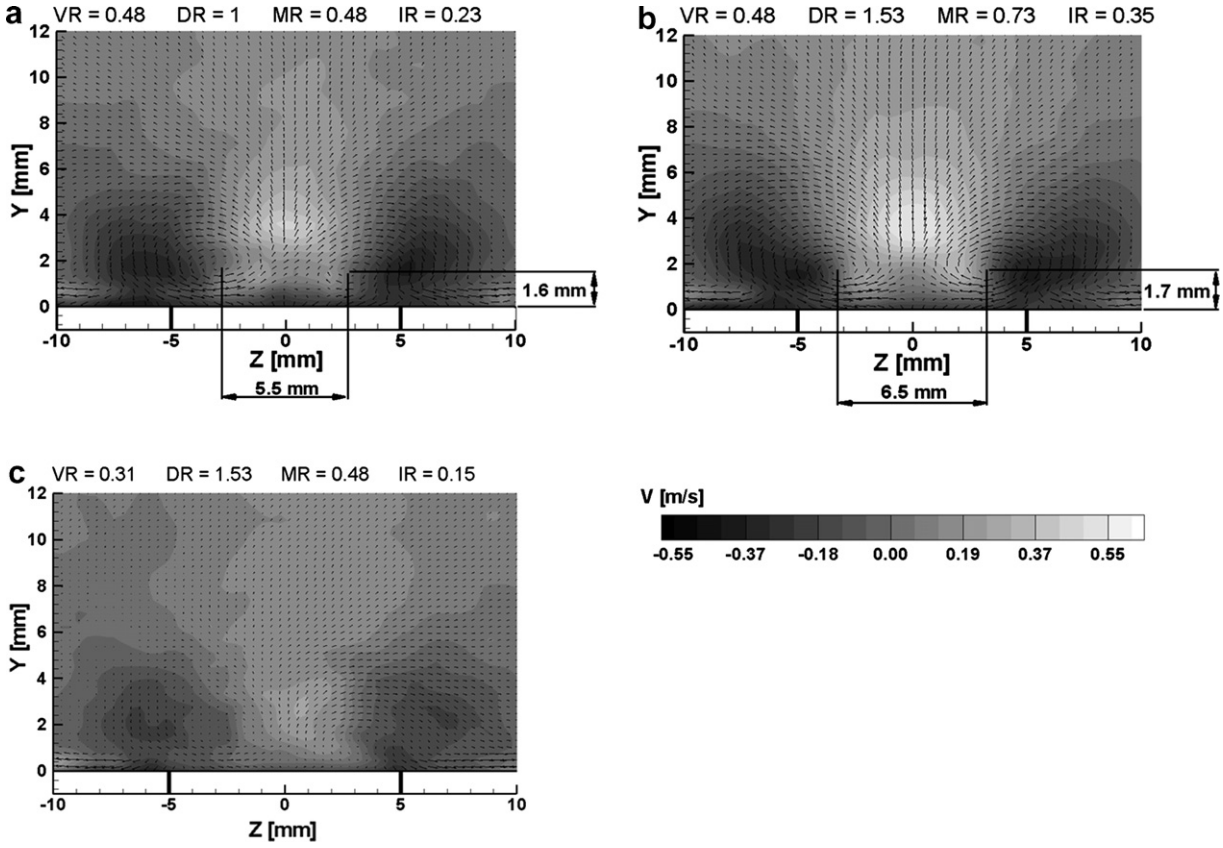

Fig. 11. Normal velocity contours and velocity field in the Y–Z-plane perpendicular to the wall at $X/D = 1.75$, air injection at VR = MR = 0.48 (a), CO_2 injection at VR = 0.48 (b) and CO_2 injection at MR = 0.48 (c).

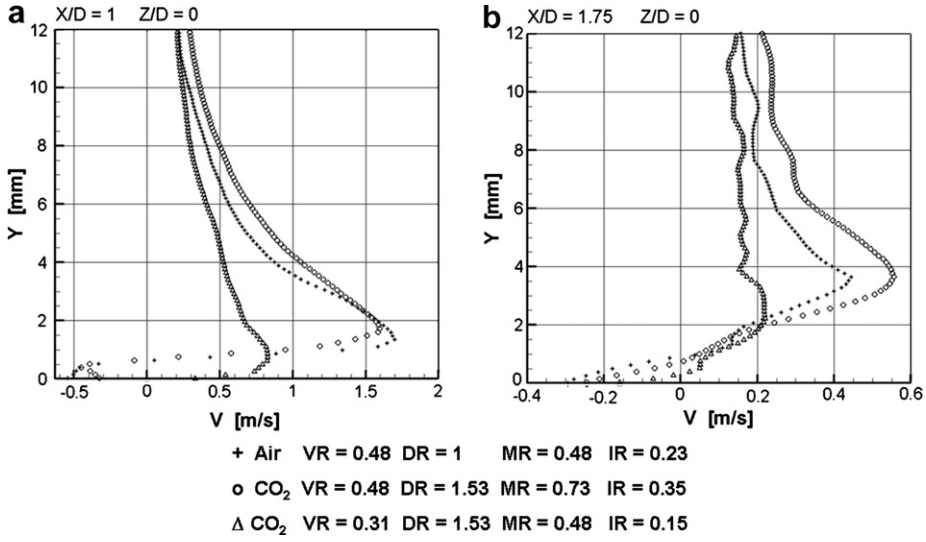

Fig. 12. Normal velocity profiles along the centerline at $X/D = 1$ (a) and $X/D = 1.75$ (b) for air and CO_2 injections at VR = 0.48 and MR = 0.48.

The illustrations demonstrate the crucial effect of the density on the film jet spreading downstream of the exit hole, which is important for the cooling performance, and confirm analogous findings by Sinha et al. (1991).

6. Comparison with numerical results

The experimental results of the present study are used to validate the large-eddy simulations (LES) that are performed by Renze et al. (in press) to investigate the jet-in-a-crossflow (JICF). A detailed description of the LES method and the boundary conditions can be found in Guo et al. (2006). The LES method for different jet fluids is specified in Renze et al. (2007). LES of turbulent mixing with different gas species is described in Renze et al. (accepted for publication).

The interaction of the turbulent boundary layer with a high density cooling jet is shown in Fig. 13. The velocity ratio is VR = 0.28 and the density ratio is DR = 1.53, which resembles the CO_2–air mass ratio. The Fig. 13a displays the JICF part of the computational domain. The velocity field is emphasized by streamlines to show the

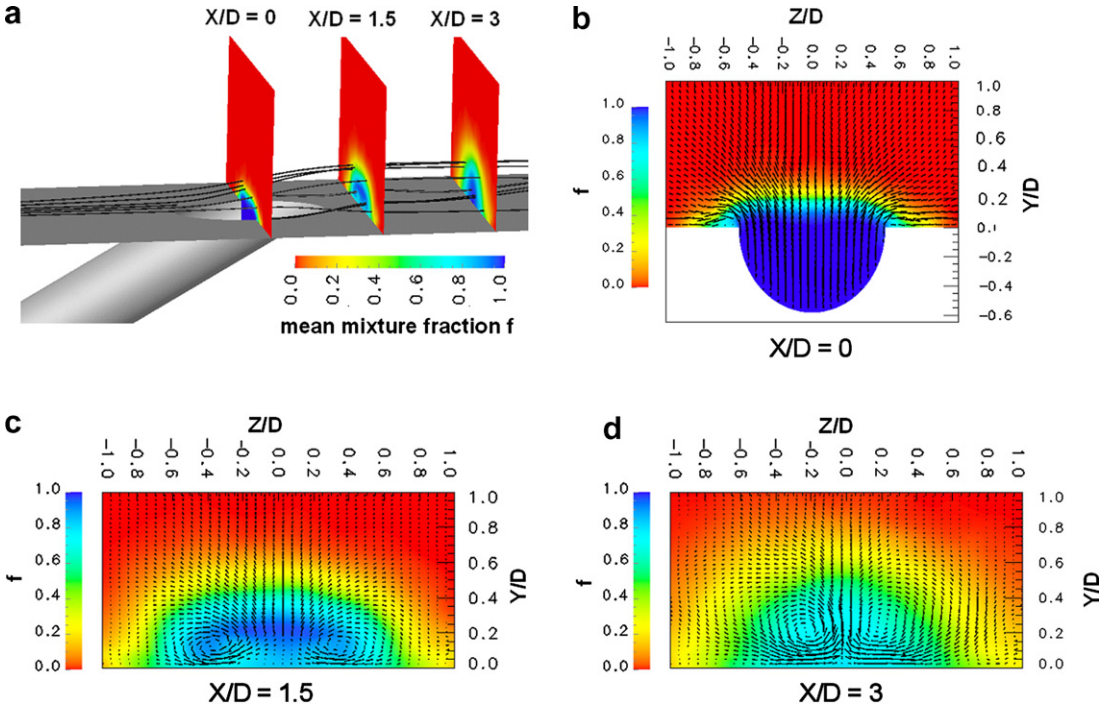

Fig. 13. Large-eddy simulations at VR = 0.28 and DR = 1.53, streamlines and contours of the mixture fraction f at different cross sections (a), contours of the mixture fraction f and velocity vectors in the cross section at $X/D = 0$ (b), cross section at $X/D = 1.5$ (c) and cross section at $X/D = 3$ (d).

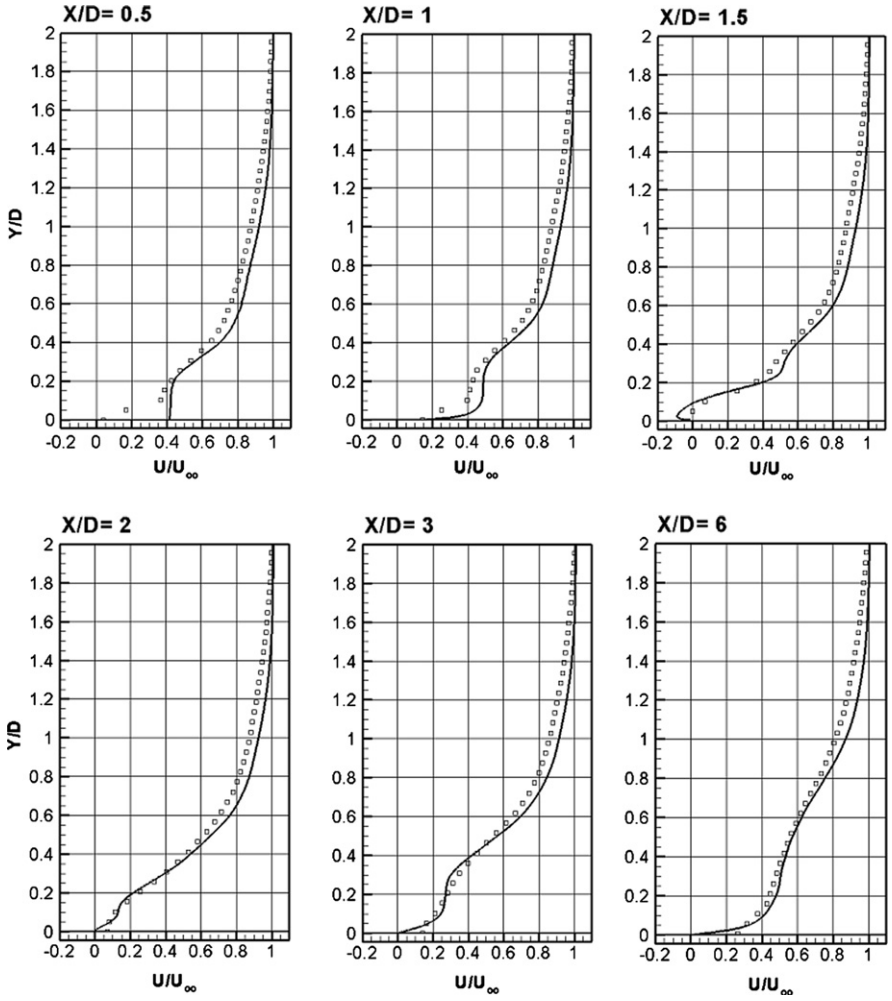

Fig. 14. Streamwise velocity profiles of CO_2 injection in the symmetry plane at different streamwise locations at VR = 0.28, PIV data: □, LES data: solid line.

deflection of the crossflow by the jet and the swirling motion of the jet fluid being entrained by the crossflow. Furthermore, contours of the mean mixture fraction $f = \rho_n/\rho_{tot}$ of the jet fluid are shown in several cross sections at different X/D locations.

The cross sections are enlarged and vectors to evidence the secondary velocity field are added. At $X/D = 0$ the high density fluid starts to penetrate into the crossflow and the shear layers start to roll up at the jet hole edges (Fig. 13b). At $X/D = 1.5$ the counter-rotating vortex pair (CVP) resulting from the shear between the jet and the crossflow fluid (Renze et al., 2007) is already fully developed (Fig. 13c). The mixing between both fluids follows the development of the vortex pair. The maximum values of the mixture fraction f mark the centers of the vortices of the unmixed jet fluid. They are lifted off the wall as low density fluid from the crossflow is entrained between the wall and the jet by the CVP. The cross section at $X/D = 3$ shows the streamwise development CVP which continuously grows (Fig. 13d). The vorticity magnitude is decreased, the centers of the CVP approach each other and drift away from the surface.

In Fig. 14 profiles of the streamwise velocity component are compared for the CO_2 jet at VR = 0.28. The distributions are located in the spanwise symmetry plane ($Z/D = 0$) at different streamwise locations ($X/D = 0.5$, 1, 1.5, 2, 3 and 6). The location $X/D = 0.5$ corresponds to the leeward part of the injection hole exit where the CO_2 jet penetrates into the boundary layer. At $X/D = 1$ the boundary layer is lifted by the emanating jet. The jet separates at $X/D = 1.5$ and reattaches at $X/D = 2$. Even at $X/D = 3$ and $X/D = 6$ the velocity profiles show the clear impact of the jet injection, which is evidenced by the deviation from the velocity profile of a fully developed turbulent boundary layer. The numerically predicted flow is in good agreement with the PIV measurements, although a slight quantitative disagreement is visible. Especially in the outer region the PIV measurements predict a smaller velocity than the LES. The maximum deviation of the PIV and LES profiles is in the range of 10%. This mismatch

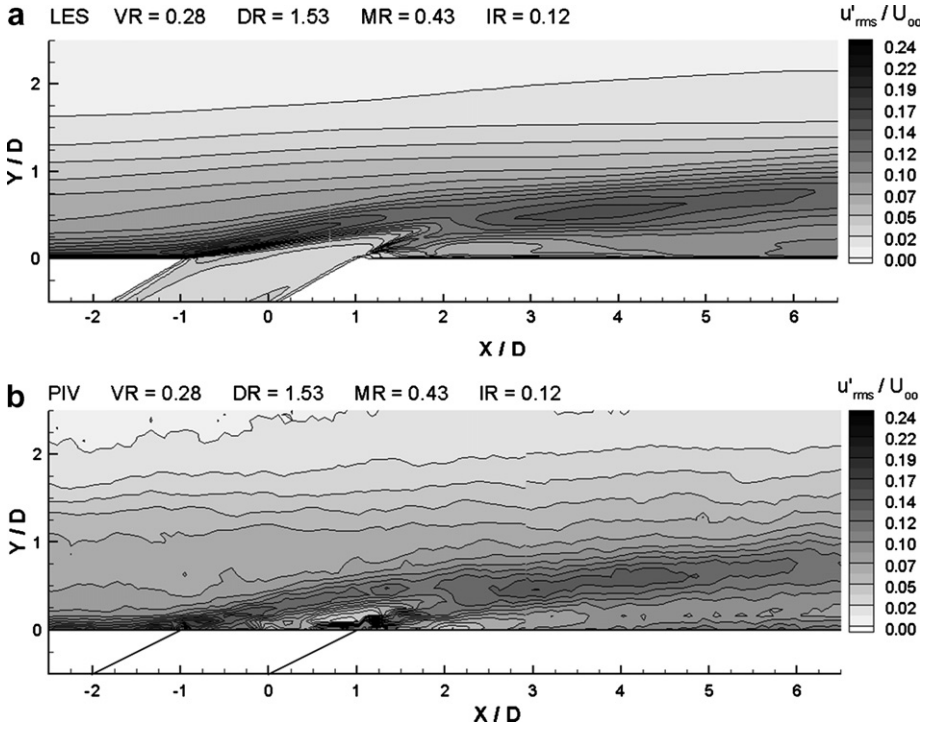

Fig. 15. Contours of the streamwise turbulence intensity u'_{rms}/u_∞ at VR = 0.28 for CO_2 injection, (a) LES, (b) PIV.

could be due to the different boundary condition in the outer flow field. That is, in the LES no freestream turbulence is introduced, i.e., the freestream turbulence of 0.1% in the wind tunnel flow is not taken into account in the numerical analysis. This turbulence level has been determined by hot wire measurements in the freestream above a flat plate.

Contours of streamwise turbulence intensity u'_{rms}/u_∞ are illustrated in Fig. 15. A cross section in the spanwise symmetry plane at VR = 0.28 and DR = 1.53 is shown. The peak values of the velocity fluctuations u'_{rms} are located in the shear zone between the crossflow and the jet, which emanates from the leading edge of the jet hole. This area corresponds to the lifted turbulent boundary layer, starting to interact with the crossflow. Pronounced fluctuations can also be found in the recirculation zone at the trailing edge of the hole. In this region of high turbulence a pronounced mixing between the jet and the crossflow occurs. The comparison of the PIV results averaged over 400 pictures and the numerical findings averaged over 800 time samples show the data to be in excellent qualitative agreement.

Distributions of the streamwise turbulence intensity u'_{rms}/u_∞ are illustrated at several streamwise locations ($X/D = -1$, $X/D = 1$, $X/D = 1.5$, $X/D = 2$ $X/D = 3$ and $X/D = 6$) in Fig. 16. The profiles at $X/D = -1$ correspond to the upstream edge of the jet hole where the boundary flow is undisturbed. The peak values at $X/D = 1$ evidence the displacement of the boundary layer due to the emanating jet. Overall, the PIV and LES predictions of the higher moment velocity distributions do agree convincingly. Nevertheless, it must be noted that locally a deviation of approximately 20% occurs. Discrepancies occur below $Y/D = 0.05$ are caused by the laser light pulse distance in the PIV settings. The pulse distance is chosen to achieve a high resolution over a wide range of the boundary layer. Due to the fact that the velocity gradients are very high in the near-wall region it is difficult to choose an adequate pulse distance that covers the whole boundary layer, i.e., a pulse distance equally well for the outer boundary layer flow and the flow close to the wall. At $X/D = 1.5$ the peak turbulence levels occur in the lifted regions at $Y/D = 0.5$ and in the recirculation zone at about $Y/D = 0.2$. At $X/D = 2$ both peak level zones are merged and the distribution possesses a strong deviation from the customary distribution inside a turbulent boundary layer. Further downstream at $X/D = 3$ and $X/D = 6$ the high turbulence level has shifted away from the wall into the boundary layer, where the counter-rotating vortex pair, which governs the mixing process downstream of the jet hole, is fully developed.

Due to the investigation of the flow field using the PIV technique the cooling effectiveness is not directly measured. However, the influence of the density ratio on the cooling effectiveness is determined from the experimentally validated LES data. The distribution of the CO_2 mixture fraction f along a flat plate at a velocity ratio of VR = 0.28 and a mass flux ratio MR = 0.43, respectively, is given in Fig. 17. The graph shows the mean mixture fraction in the spanwise symmetry plane as a function of the streamwise coordinate. The data is compared with the findings of Sinha et al. (1991).

The symbols represent the measured film-cooling effectiveness η, which is a temperature based variable, at a

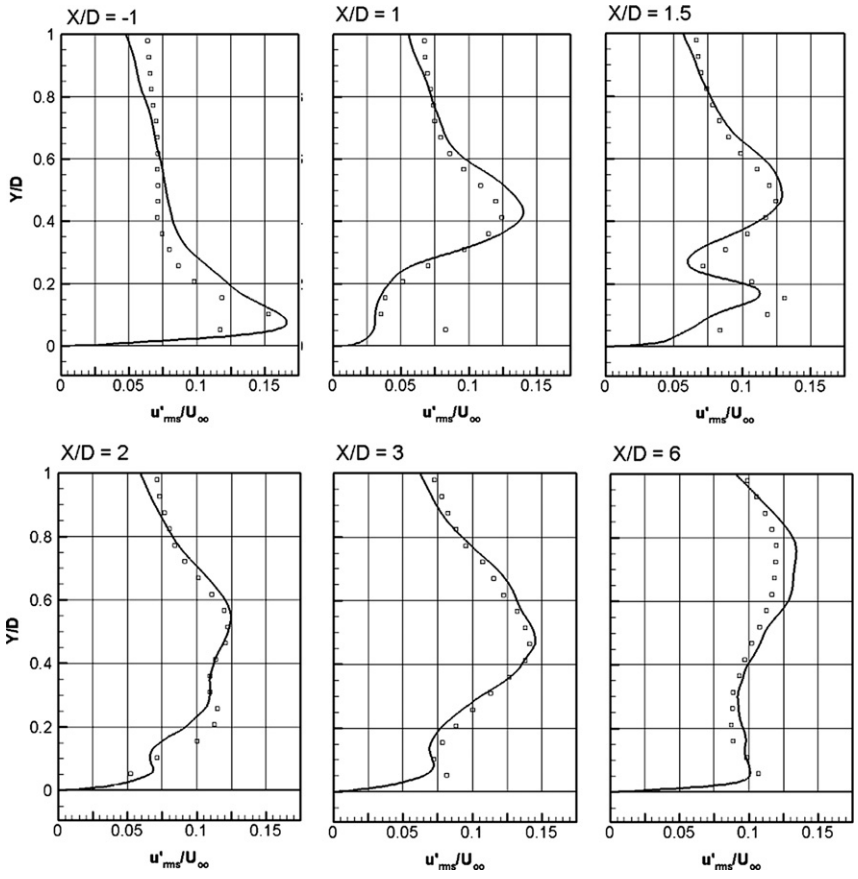

Fig. 16. Distributions of the streamwise turbulence intensity u'_{rms}/u_∞ at VR = 0.28 for CO_2 injection, PIV data: □, LES data: solid line.

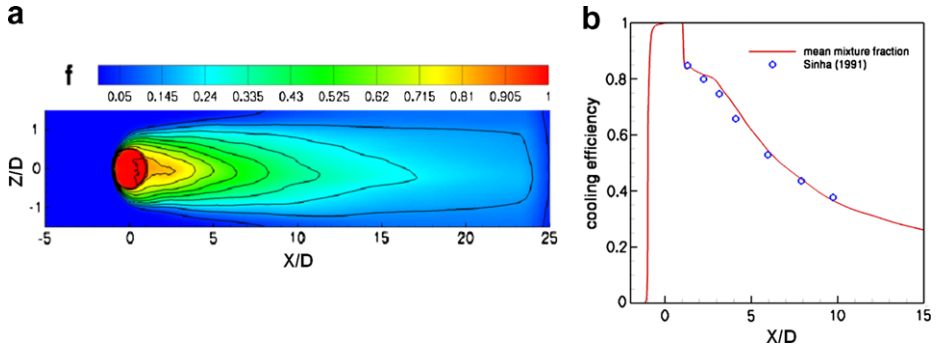

Fig. 17. Contours of mean mixture fraction along the flat plate (a), mean mixture fraction in the spanwise symmetry plane compared with the cooling efficiency by Sinha et al. (1991) (b).

slightly different mass flux ratio of MR = 0.5. The good agreement between both curves show the mixture friction distribution along the plate to correctly predict the film-cooling efficiency of such flow configurations.

7. Conclusions

The velocity fields of inclined jets in a crossflow have been experimentally investigated using the PIV technique. To simulate the impact of the density ratio between the coolant and the mainstream, air and CO_2 were separately injected into the crossflow of air. The results show that a higher velocity ratio enlarges the size of the recirculation region leading to a more pronounced entrainment of crossflow fluid into the wake of the jet.

Velocity effects dominate the flow field in the vicinity of the jet hole. However, the lateral spreading of the coolant downstream, which is crucial for the cooling efficiency, is strongly increased at a higher density ratio. Furthermore, the comparison of experimentally and numerically

determined distributions of the mean streamwise velocity and the higher moments shows a very good qualitative and quantitative agreement.

Acknowledgement

The support of this research by the Deutsche Forschungsgemeinschaft (DFG) in the frame of the SFB 561 is gratefully acknowledged.

References

Baldauf, S., Schulz, A., Wittig, S., 2001. High-resolution measurements of local effectiveness from discrete hole film cooling. ASME Journal of Turbomachinery 123, 758–765.

Bernsdorf, S., Rose, M.G., Abhari, R.S., 2006. Modeling of film cooling – Part I: Experimental study of flow structure. ASME Journal of Turbomachinery 128, 141–149.

David, L., Fraticelli, R., Calluaud, D., Boreé, J., 2004. Cross flow investigation by stereoscopic PIV measurements. In: 12th International Symposium on Application of Laser Techniques to Fluid Mechanics, Lisbon.

Ekkad, S.V., Zapata, D., Han, J.C., 1997. Heat transfer coefficients over a flat surface with air and CO_2 injection through compound angle holes using a transient liquid crystal image method. ASME Journal of Turbomachinery 119, 580–586.

Ekkad, S.V., Han, J.C., Du, H., 1998. Detailed film cooling measurements on a cylindrical leading edge model: effect of free-stream turbulence and coolant density. ASME Journal of Turbomachinery 120, 799–807.

Goldstein, R.J., Eckert, E.R.G., 1974. Effects of hole geometry and density on three-dimensional film cooling. International Journal of Heat Mass Transfer 17, 595–607.

Guo, X., Schröder, W., Meinke, M., 2006. Large-eddy simulations of film cooling flows. Computers and Fluids 35 (6), 587–606.

Han, J.C., Mehendale, A.H., 1986. Flat plate film cooling with steam injection through one row and two rows of inclined holes. ASME Journal of Turbomachinery 108, 137–144.

Jovanovic, M.B., de Lange, H.C., van Steenhoven, A.A., 2006. Influence of hole imperfection on jet cross flow interaction. International Journal of Heat and Fluid Flow 27, 52–53.

Kohli, A., Bogard, D.G., 2005. Turbulent transport in film cooling flows. Journal of Turbomachinery 127, 513–520.

Mehendale, A.B., Han, J.C., Ou, S., Lee, C.P., 1994. Unsteady wake over a linear turbine blade cascade with air and CO_2 film injection: Part II – Effect on film effectiveness and heat transfer distributions. ASME Journal of Turbomachinery 116, 730–737.

Meinhart, C.D., Barnhart, D.H., Adrian, R.J., 1994. An interrogation and vector validation system for holographic particle image fields. In: 7th International Symposium on Applications of Laser Techniques to Fluid Mechanics, Lisbon, pp. 1.4.1–1.4.6.

Peterson, S.D., Plesniak, M.W., 2004. Evolution of jets emanating from short holes into crossflow. Journal of Fluid Mechanics 503, 57–91.

Petersen, D.R., Eckert, E.R.G., Goldstein, R.J., 1977. Film cooling with large density differences between the mainstream and the secondary fluid measured by heat-mass transfer analogy. Journal of Heat Transfer 99, 620–627.

Pietrzyk, J.R., Bogard, D.G., Crawford, M.E., 1990. Effects of density ratio on the hydrodynamics of film cooling. ASME Journal of Turbomachinery 112, 437–443.

Raffel, M., Kompenhans, J., Willert, C.E., 1998. Particle Image Velocimetry. Springer-Verlag, Berlin Heidelberg New York.

Renze, P., Meinke, M., Schröder, W., 2007. Large-eddy simulation of film cooling for different jet fluids. Journal of Aerospace Power 22, 10.

Renze, P., Meinke, M., Schröder, W., in press. Large-eddy simulation of film cooling flows with variable density jets. Journal of Flow, Turbulence and Combustion.

Renze, P., Meinke, M., Schröder, W., accepted for publication. Large-eddy simulation of film cooling flows at density gradients. International Journal of Heat and Fluid Flow.

Sinha, K., Bogard, D.G., Crawford, M.E., 1991. Film cooling effectiveness downstream of a single row of holes of variable density ratio. ASME Journal of Turbomachinery 113, 442–449.

Teekaram, A.J.H., Fort, C.J.P., Jones, T.V., 1989. The use of foreign gas to simulate the effects of density ratios in film cooling. ASME Journal of Turbomachinery 111, 57–62.

Walters, D.K., Leylek, J.H., 2000. A detailed analysis of film cooling physics: Part I – Streamwise injection with cylindrical holes. ASME Journal of Turbomachinery 122, 102–112.